Boise State University

ScholarWorks

1-2018

Atomic Layer Deposition of Molybdenum Disulfide Films Using MoF$_6$ and H$_2$S

Steven Letourneau
Boise State University

Elton Graugnard
Boise State University

Atomic layer deposition of molybdenum disulfide films using MoF$_6$ and H$_2$S

Anil U. Mane
Energy Systems Division, Argonne National Laboratory, 9700 S. Cass Ave., Argonne, Illinois 60439

Steven Letourneau
Micron School of Materials Science and Engineering, Boise State University, 1910 University Dr., Boise, Idaho 83725

David J. Mandia
Energy Systems Division, Argonne National Laboratory, 9700 S. Cass Ave., Argonne, Illinois 60439

Jian Liu
Department of Chemistry, Northwestern University, 2145 Sheridan Rd., Evanston, Illinois 60208

Joseph A. Libera, Yu Lei, and Qing Peng
Energy Systems Division, Argonne National Laboratory, 9700 S. Cass Ave., Argonne, Illinois 60439

Elton Graugnard
Micron School of Materials Science and Engineering, Boise State University, 1910 University Dr., Boise Idaho 83725

Jeffrey W. Elam[a)]
Energy Systems Division, Argonne National Laboratory, 9700 S. Cass Ave, Argonne, Illinois 60439

Molybdenum sulfide films were grown by atomic layer deposition on silicon and fused silica substrates using molybdenum hexafluoride (MoF$_6$) and hydrogen sulfide at 200 °C. *In situ* quartz crystal microbalance (QCM) measurements confirmed linear growth at 0.46 Å/cycle and self-limiting chemistry for both precursors. Analysis of the QCM step shapes indicated that MoS$_2$ is the reaction product, and this finding is supported by x-ray photoelectron spectroscopy measurements showing that Mo is predominantly in the Mo(IV) state. However, Raman spectroscopy and x-ray diffraction measurements failed to identify crystalline MoS$_2$ in the as-deposited films, and this might result from unreacted MoF$_x$ residues in the films. Annealing the films at 350 °C in a hydrogen rich environment yielded crystalline MoS$_2$ and reduced the F concentration in the films. Optical transmission measurements yielded a bandgap of 1.3 eV. Finally, the authors observed that the MoS$_2$ growth per cycle was accelerated when a fraction of the MoF$_6$ pulses were substituted with diethyl zinc. *Published by the AVS.* https://doi.org/10.1116/1.5003423

I. INTRODUCTION

Research on layered materials, such as two-dimensional (2D) transition metal dichalcogenides (TMDCs), has grown rapidly in the past decade. After the mechanical exfoliation of graphene was reported in 2004,[1] numerous new 2D materials have been synthesized and researched.[2,3] Prior to this recent interest in TMDCs, 2D materials such as molybdenum disulfide (MoS$_2$) and tungsten disulfide (WS$_2$) were used primarily as solid state lubricants.[4] These materials have layered structures and were heavily researched in their bulk (multilayer), nanotube, and fullerene structural forms.[5] More recently, the unique optical and electrical properties of these materials[2,6] have attracted much attention, with MoS$_2$ quickly becoming the prototypical TMDC. Whereas bulk MoS$_2$ has a band gap of 1.3 eV, single monolayer MoS$_2$ has a unique indirect-to-direct band gap transition of 1.8 eV.[6] This presents a unique opportunity for semiconductor device manufacturing compared to the more widely studied graphene which is metallic (no bandgap) in its native state. MoS$_2$ has also been used as a cathode and anode barrier layer in lithium ion batteries[7,8] and as a catalyst for hydrogen production.[9,10]

A. Structure and composition

Transition metal dichalcogenides (MX$_2$ where M is a transition metal and X is a chalcogenide) have a layered structure where each layer consists of an X-M-X unit. The TMDC crystals are typically described as having trigonal or octahedral prismatic coordination to help describe the material in a single layer, where each M atom has six X atoms forming a hexagon above and below it.[11,12] These atomic tri-layers feature strong in-plane covalent bonding, but weak van der Waals bonding between layers. This dichotomy of bonding characteristics facilitates the synthesis and isolation of single layer TMDCs. MoS$_2$ in the bulk crystalline form has three stable phases under standard conditions: 2H, 3R and 1T.[13,14] While the 2H and 3R are of the most interest because of their indirect-to-direct bandgap transition, the 1T phase has received less attention in the electronics field because its metallic properties are not suitable for devices such as transistors.

B. Coatings and growth

Two-dimensional MoS$_2$ has been synthesized using a variety of top-down and bottom-up methods. Typical top-down methods are mechanical exfoliation,[1] liquid exfoliation,[15]

[a)]Electronic mail: jelam@anl.gov

and ion intercalation.[16] These methods can yield high quality monolayer films up to 2.25 μm^2 from bulk crystals.[17] Liquid exfoliation has been used to create dispersions of monolayer MoS_2 for inkjet printing flexible electronics.[18] Many bottom-up approaches have been used for coating materials, including MoS_2. Muratore *et al.* deposited three- and five-layer MoS_2 at 350 °C using physical vapor deposition showing little to no oxygen contamination during growth.[19] Wu *et al.* synthesized high quality MoS_2, WS_2, and multilayer films by the sequential sulfurization of Mo and W metal for vertical heterostructures.[20] Using chemical vapor deposition (CVD), Vilá *et al.* controlled the orientation of the MoS_2 growth by varying the MoO_x:S_2 ratio while sulfurizing MoO_3 at 750 °C.[21] Feng *et al.* controlled the grain size of single layer MoS_2 by controlling the H_2 with MoO_3 and elemental sulfur.[22] In addition to the oxide, $MoCl_5$ and elemental sulfur have been used to grow monolayer MoS_2 at high temperatures.[23] Among the various bottom-up approaches for growing MoS_2 thin films, atomic layer deposition (ALD) holds great appeal since the layer-by-layer growth has the potential to create uniform monolayer MoS_2 over large areas.

C. ALD of MoS$_2$

ALD is a chemical vapor process that involves sequential pulses of precursor vapors and is defined by self-limiting surface half-reactions.[24] Tan *et al.* showed ALD of MoS_2 using $MoCl_5$ and H_2S, which yielded a continuous film after 10 cycles at 300 °C.[25] Crystalline monolayers were obtained after annealing at high temperatures. Using this same chemistry, Browning *et al.* showed similar growth and used this method to fabricate back-gated field effect transistors. They found a relatively low mobility of $1 \, cm^2 \, V^{-1} \, s^{-1}$, which they attributed to their device geometries.[26] Valdivia *et al.* reported the ability to grow MoS_2 on 150 mm Si/SiO_2 substrates.[27] Molybdenum carbonyl [$Mo(CO)_6$] has been used by multiple groups in conjunction with H_2S.[8,28,29] Jin *et al.* grew amorphous MoS_2 films with $Mo(CO)_6$ and dimethyldisulfide at 100 °C.[30] Recently, Jurca *et al.* reported a low-temperature ALD process using $Mo(NMe_2)_4$ and H_2S between 60 and 120 °C, while Mattinen *et al.* reported a process using a new Mo precursor with H_2S to deposit films between 250 and 350 °C that exhibited a range of morphologies and crystallinity.[31,32] For both of these studies, deposition at higher temperatures resulted in decomposition of the Mo precursor and non-self-limiting growth. Among the ALD MoS_2 publications to date, those that report 2D films are Refs. 25–30.

Scharf *et al.* reported that WS_2 ALD using tungsten hexafluoride (WF_6) and H_2S did not grow on the native oxide of silicon but readily nucleated on ALD ZnS.[33] Interestingly, the ALD WS_2 growth per cycle (GPC) decreased steadily with increasing WS_2 thickness on the ALD ZnS surface, but the higher initial WS_2 GPC was easily restored using a single pulse of diethyl zinc (DEZ).[33] Delabie *et al.* obtained WS_2 films by depositing a Si sacrificial layer on top of Al_2O_3 to aid in the reduction of the WF_6.[34] In addition to the sacrificial layer, a H_2 plasma was used after the WF_6 dose, which

yielded a crystalline WS_2 film without the need for postdeposition annealing.[34]

In this study, we explored MoS_2 ALD using molybdenum fluoride (MoF_6) and H_2S. MoF_6 has been used previously for Mo ALD using disilane,[35] and for MoS_2 CVD with H_2S.[36,37] MoF_6 is reduced readily by both Si and H_2 (Ref. 38),

$$2MoF_6(g) + 3Si(s) \rightarrow 2Mo(s) + 3SiF_4(g), \tag{1}$$

$$MoF_6(g) + 3H_2(g) \rightarrow Mo(s) + 6HF(g). \tag{2}$$
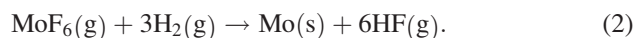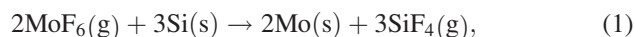
The free energy changes for these reactions are −450 and −237 kJ/mol Mo, respectively, at 200 °C, indicating that both reactions are thermodynamically highly favorable.[38] In the previous report of Mo ALD using MoF_6 and disilane, the authors reported self-limiting behavior but measured a higher than predicted GPC which they attributed to CVD (i.e., $MoF_6 \rightarrow Mo + 3F_2$) promoted by local, transient heating from the very exothermic ALD surface reactions.

In, this work x-ray amorphous molybdenum sulfide films were grown by ALD using MoF_6 and H_2S. *In situ* quartz crystal microbalance (QCM) measurements revealed that both half-reactions are self-limiting at 200 °C. Crystalline films were achieved after annealing at 350 °C in a hydrogen environment. The growth rate could be enhanced using diethyl zinc without changing the optical band gap of the material.

II. EXPERIMENT

A. Growth

MoS_2 ALD was performed using a custom viscous flow, hot-walled reactor, which was detailed previously.[39] Deposition was performed on ∼1 × 1 in. coupons of Si with the native oxide intact and fused silica. The reactor temperature was maintained at 200 °C for all samples. During growth, ultrahigh purity N_2 (99.999%) was adjusted so the system process pressure was approximately 1 Torr. Molybdenum hexafluoride (MoF_6 98%, Sigma Aldrich) and hydrogen disulfide (H_2S 99.5% Matheson Trigas) were sequentially pulsed into the reactor with purges of N_2 between each exposure. The MoF_6 and H_2S partial pressures were 20 and 150 mTorr during dosing of the respective precursor. The delivery pressure in the reactor for both precursors was regulated with both an inline 200 μm aperture (Lenox Laser) and a metering valve. Both gases are extremely dangerous and special precautions are needed due to the flammability/toxicity of H_2S and the corrosive nature of MoF_6. The ALD timing can be described as t_1-t_2-t_3-t_4, where t_1 and t_3 are the MoF_6 and H_2S exposure times, respectively, and t_2 and t_4 are the corresponding purge times with all times in seconds (s). For the MoS_2 growth, t_1 and t_3 were both 1 s, while the purge times (t_2 and t_4) were kept at 5 s. In some experiments, the samples were annealed *in situ* after deposition on a temperature-controlled hot stage. The sample annealing was performed in ultrahigh purity hydrogen at 350 °C holding for 15 min. The samples were then cooled quickly back to room temperature. In addition to the binary chemistry of MoF_6 and H_2S, the MoS_2 ALD was

promoted/doped with ZnS using two successive ZnS ALD cycles composed of DEZ (99% Sigma Aldrich) and H_2S.

B. Characterization

The MoS_2 ALD was investigated by *in situ* QCM measurements using a modified Maxtek Model BSH-150 sensor head. An RC cut quartz crystal (Phillip Technologies) with an alloy coating was used as the sensor due to its broad temperature range. To prevent deposition on the back side of the crystal, silver paste was used to seal the crystal and sensor head.[39] A backside N_2 purge was adjusted to approximately 0.5% of the process pressure.

X-ray photoelectron spectroscopy (XPS) measurements were carried out at the KECKII/NUANCE facility at Northwestern University on a Thermo Scientific ESCALAB 250 Xi (Al Kα radiation, hν = S5 1486.6 eV) equipped with an electron flood gun. Lower resolution survey scans and high resolution scans of the 3d, 2s and 2p electron energies were performed. The XPS data were analyzed using THERMO AVANTAGE 5.97 software and all spectra were referenced to the C1s peak (284.8 eV). Peak deconvolution in the high-resolution spectra (Mo 3d, S 2p) was performed using the Powell fitting algorithm with 30% mixed Gaussian–Lorentzian fitted peaks in all cases. Fitting procedures were based on constraining the spin-orbit split doublet peak areas and FWHM according to the relevant core level (e.g., $3d_{5/2}$ and $3d_{3/2}$ is constrained to 3:2 peak area).

Raman spectroscopy (inVia, Renishaw) was used to probe the layered structure. The E_{2g} and A_{1g} vibrational modes arise from the in-plane and out-of-plane modes, respectively.[40] Measurements were performed in reflection using an excitation wavelength of 514 nm on all samples. To prevent sample damage, a neutral density filter of 5%–10% transmission was used. A D2 Phaser x-ray diffractometer (XRD) (Bruker) using a Cu Kα source in Bragg-Brentano geometry was used to probe the crystallinity and crystal structure of the MoS_2. A J.A. Woollam, Inc. α-SE Ellipsometer (Lincoln, NE) was used to measure the thickness of the bulk films using a Cauchy model.
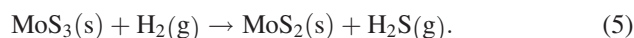
The optical properties of the ALD molybdenum sulfide were measured using a Cary 5000 spectrophotometer (Varian) in transmission mode on films deposited on fused silica substrates. Kapton tape was placed on the backside of the quartz substrates during ALD and removed prior to measurement to mask off the region probed by the Cary 5000 beam. Prior to each measurement, a background reference was recorded to ensure accuracy. Linear regression of Tauc-plots was used to determine the optical band-gap of the films.

III. RESULTS AND DISCUSSION

A. QCM of MoF_6 + H_2S

Thermodynamic calculations (HSC Chemistry, Outotec Oy) of the Gibbs free energies of reaction (ΔG) were performed to evaluate possible chemical reactions occurring during the molybdenum sulfide ALD. Two plausible chemical pathways were identified: direct and indirect. In the direct pathway, MoF_6 and H_2S react to form MoS_2, HF, and

elemental S [Eq. (3)], with $\Delta G = -379$ kJ/mol at 200 °C. In the indirect pathway, the initial solid-phase product is MoS_3 [Eq. (4)], with $\Delta G = -402$ kJ/mol at 200 °C. Subsequent H_2 reduction [Eq. (5)] yields MoS_2, with $\Delta G = -24$ kJ/mol at 350 °C. [We compute ΔG at 350 °C for Eq. (5) to match the experimental conditions used in the postdeposition annealing]. We note that the indirect pathway has a greater thermodynamic driving force ($\Delta G = -426$ kJ/mol) compared to the direct pathway ($\Delta G = -379$ kJ/mol). Moreover, the direct pathway might have a larger activation energy given the requirement for Mo reduction (+6 to +4) in Eq. (3), and so the indirect pathway might be kinetically favored as well. These mechanistic considerations will come into play later in our data analysis.

$$MoF_6(g) + 3H_2S(g) \rightarrow MoS_2(s) + 6HF(g) + S(s), \quad (3)$$

$$MoF_6(g) + 3H_2S(g) \rightarrow MoS_3(s) + 6HF(g), \quad (4)$$

$$MoS_3(s) + H_2(g) \rightarrow MoS_2(s) + H_2S(g). \quad (5)$$

Our initial QCM studies were performed to probe the degree of self-limitation for the MoF_6 and H_2S half-reactions. Figure 1(a) shows the *in situ* QCM measurements (red circles) recorded using the timing sequence x–5-1-5 where the MoF_6 exposure time was varied between $x = 0$–2 s. The growth per cycle values were calculated assuming a bulk density of MoS_2, $d = 5.06$ g/cm^3. The QCM data were fit with a Langmuir adsorption curve (line) and demonstrate saturation after ~1 s MoF_6 exposure time at 0.4 Å/cycle. These measurements were repeated using the timing sequence 1-5-x-5 where the H_2S exposure time was varied between $x = 0$–2 s and revealed saturation after ~1 s H_2S exposures at 0.40 Å/cycle [Fig. 1(b)]

Next, we used *in situ* QCM to monitor the mass changes versus time during molybdenum sulfide ALD using the timing sequence 1.5–15-1.5–15 at 200 °C [Fig. 2(a)]. The MoF_6 and H_2S dosing periods are indicated by the red and blue traces, respectively, at the bottom of the graph. We found linear growth at a GPC of 0.46($\pm$0.01) Å/cycle using $d = 5.06$ g/cm^3. This value is slightly higher than the GPC value of 0.40 Å/cycle from Fig. 1 and this discrepancy may relate to the longer dose times of 1.5 s used for both precursors in Fig. 2(a) while in Fig. 1 one of the precursor dose times was fixed at 1.0 s.

The data in Fig. 2(a) show a regular staircase pattern that coincides with the precursor dosing times. Figure 2(b) shows a magnified view of the QCM data for the first two ALD cycles. We see that the thickness (or mass) increases abruptly during the MoF_6 exposures and decreases abruptly during the H_2S exposures. Furthermore, the mass decreases continuously during the MoF_6 purge periods and appears to approach a steady-state value. In contrast, the mass is constant during the H_2S purge times. The slight delay between the QCM response and the precursor dosing traces results from the transit time of ~0.5 s required for the precursors to travel from the dosing valves to the QCM in our ALD system.

The relative mass changes produced by the MoF_6 and H_2S exposures can be used to evaluate the molybdenum
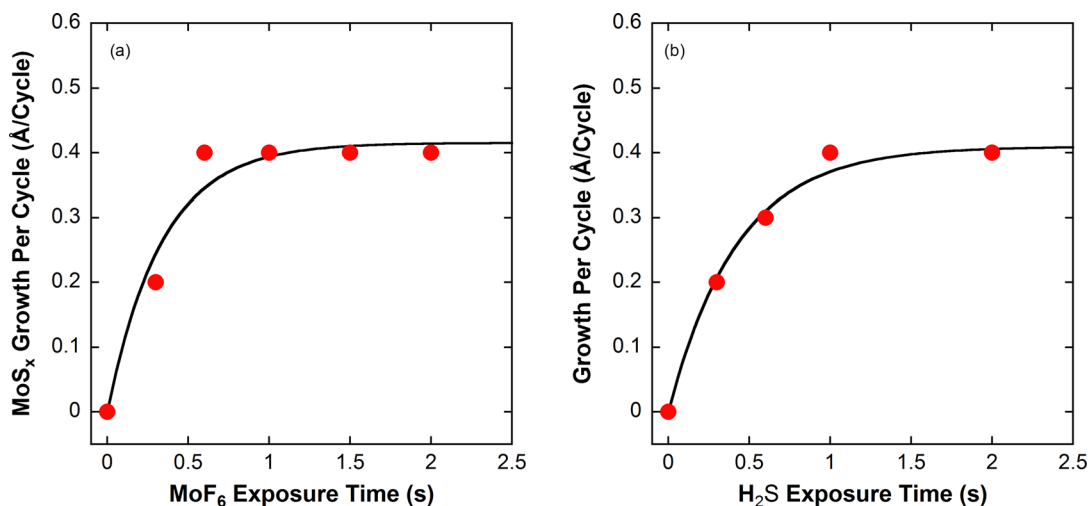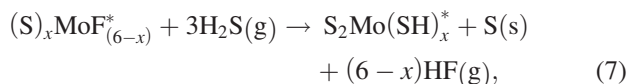
FIG. 1. (Color online) QCM data for molybdenum sulfide ALD varying (a) MoF_6 dose time and (b) H_2S dose time using 5 s purge times and a constant 1 s dose times for the other precursor in both cases. Prior to these measurements, MoF_6 and H_2S were pulsed using a 1.5-15-1.5-15 timing sequence until steady state growth was achieved.

sulfide growth mechanism. If we assume that the molybdenum sulfide ALD proceeds via the direct route [Eq. (3)] and, furthermore, that the sulfur product sublimes from the surface, then we can propose the following surface reactions:

$$(SH)_x^* + MoF_6(g) \rightarrow (S)_xMoF_{(6-x)}^* + xHF(g), \quad (6)$$

$$(S)_xMoF_{(6-x)}^* + 3H_2S(g) \rightarrow S_2Mo(SH)_x^* + S(s)$$
$$+ (6-x)HF(g), \quad (7)$$

where surface species are designated with "*," and all other species are in the gas phase. In Eq. (6), MoF_6 reacts with x surface thiol (SH) groups liberating x HF molecules, so that $(6-x)$ F atoms remain bound to the Mo. In Eq. (7) the new surface reacts with H_2S to release the remaining $(6-x)$ F atoms as HF as well as solid S. We hypothesize sulfur subsequently becomes a volatile species, probably in the form of S_8, while the surface has the newly formed MoS_2 species and is terminated with x SH groups so that the original

surface functionality is restored. We note that the hypothesis of S sublimation is reasonable given that the vapor pressure of S is $\sim$2 Torr at 200 °C.[41] We can define the QCM step ratio as $R = \Delta m_A/\Delta m$, where Δm_A is the mass change from reaction Eq. (6) and Δm is the mass change for one complete ALD cycle minus the sulfur species we assumed has entered the gas phase after the reaction. Given the atomic weights of the surface species, we can write

$$R = \Delta m_A/\Delta m = (210 - 20x)/160. \quad (8)$$

The average step ratio from the QCM data in Fig. 2(a) is $R = 1.32(\pm 0.05)$. From Eq. (8), this implies that $x = 0$, meaning that there are no surface thiols involved in the ALD process, but rather the MoF_6 reacts leaving all 6 F atoms on the surface (some of which may bond to other, nearby Mo atoms).

Alternatively, the molybdenum sulfide ALD may proceeds via the indirect route [Eq. (4)], which suggests the following half-reactions:
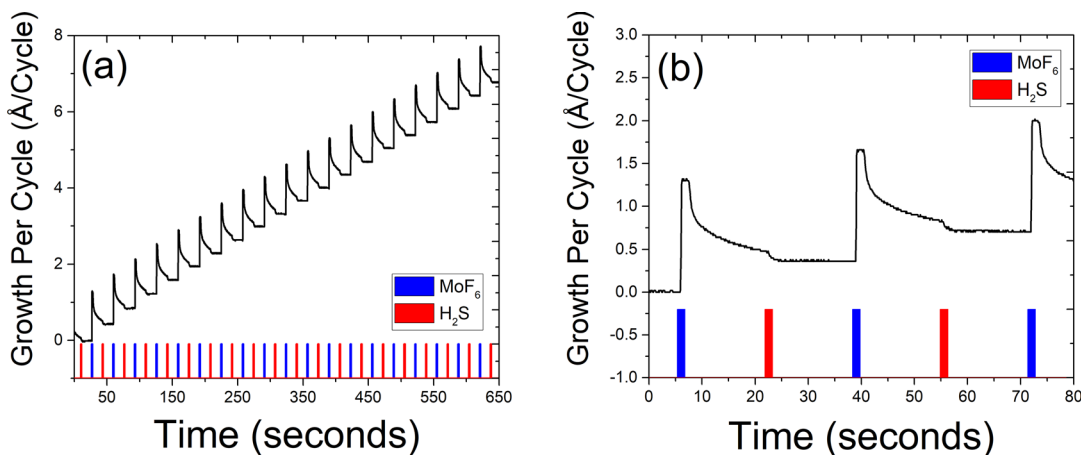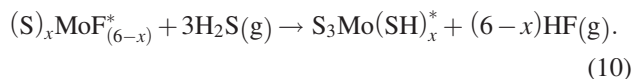

FIG. 2. (Color online) *In situ* QCM measurements during molybdenum sulfide ALD at 200 °C using the timing sequence 1.5-15-1.5-15 s over 19 ALD cycles (a) and expanded view of two successive ALD cycles (b). The MoF_6 and H_2S dosing periods are indicated at the bottom of the graphs.

$$(SH)_x^* + MoF_6(g) \rightarrow (S)_x MoF_{(6-x)}^* + xHF(g) \tag{9}$$

$$(S)_x MoF_{(6-x)}^* + 3H_2S(g) \rightarrow S_3Mo(SH)_x^* + (6-x)HF(g). \tag{10}$$

These reactions are identical to Eqs. (6) and (7) with the exception that all of the S remains on the surface and the ALD film has the composition MoS_3. Equations (9) and (10) yield the following QCM mass ratio:

$$R = \Delta M_A / \Delta M = (210 - 20x)/192. \tag{11}$$

Equation (11) predicts $R = 1.09$ for $x = 0$, and $R = 0.47$ for $x = 6$. In other words, there is no x value that yields the experimental QCM step ratio $R = 1.32(\pm 0.05)$, implying that the indirect pathway [Eq. (4)] is not correct. Given that the QCM data are consistent with the direct pathway [Eq. (3)], then a plausible interpretation for the gradual mass loss during the MoF_6 purge time is the slow sublimation of S from the surface.

B. Growth and characterization of films

A series of films were deposited on silicon and fused silica substrates using the 1–5–1–5 timing sequence at 200 °C varying the number of ALD cycles between 100 and 1000. The thicknesses of the films deposited on silicon were determined using spectroscopic ellipsometry, and these data are shown as the solid symbols in Fig. 3(a). The line in Fig. 3(a) is a quadratic fit to the thickness data and demonstrates that the thickness does not increase linearly with cycles as expected for a layer-by-layer ALD process. The thickness after 100 cycles is 60 Å and the thickness after 1000 cycles is 750 Å so that the corresponding growth per cycle values are 0.60 and 0.75 Å/cycle, respectively. Both of these values are significantly higher than the value derived from *in situ* QCM in Fig. 2(a) of 0.46 Å/cycle where only 19 cycles were performed. It is evident that the growth per cycle for the ALD MoS_2 increases with thickness. One explanation for this phenomenon can be found in the SEM image for the 600 ALD cycle film on silicon shown in Fig. 3(b). This plan-view SEM image shows a rough morphology composed of flakes with lateral dimensions of 50–100 nm and thicknesses of ~10 nm. Additional SEM images recorded at an angle of 20° to the substrate normal (not shown) indicate that these flakes extend approximately vertically from the silicon substrate surface. We hypothesize that these flakes create a surface area that increases with increasing ALD cycles and this leads to greater MoS_2 deposition. This unusual morphology might result from faster growth at the edges of the MoS_2 sheets where the ALD precursors react with defect sites.

Raman spectroscopy is a common method for identifying and characterizing MoS_2.[40] Figure 4(a) shows Raman spectra recorded from the 600 ALD cycle MoS_2 film on silicon using a 514 nm excitation laser as deposited (black line) and after the H_2 anneal (red line). The annealed MoS_2 film shows the characteristic peaks of the 2D material at 380 cm^{-1} (E_{2g}, in-plane) and 410 cm^{-1} (A_{1g}, out-of-plane). In contrast, the as-deposited film does not show these characteristic 2D MoS_2 peaks, but rather shows a weak peak at ~435 cm^{-1}. This suggests that the as-deposited films are not stoichiometric MoS_2, or that they lack short-range order.

Preannealed samples showed an amorphous film when measured by XRD; however, after annealing, MoS_2 could be seen, featuring the (002) reflection, which arises from the layered structure. The XRD data from MoS_2 are consistent with the Inorganic Crystal Structure Database PDF 01–073-1508 for the interplanar spacing.

XPS measurements were performed on both the as-deposited films and the films annealed in H_2 to investigate the chemical composition. These films were prepared using 600 ALD cycles with a thickness of 45 nm. Figure 5 shows low-resolution survey scans for the as-deposited [Fig. 5(a)] and annealed [Fig. 5(b)] films. These spectra show that F, O, Mo, and S were present in the films and the relative concentrations are given in Table I. The F detected by XPS likely results from unreacted MoF_x species in the film. We believe that the O results from exposing the substrates to air. The MoS_2 films were removed from the ALD reactor at 200 °C, and oxidation of monolayer MoS_2 has been shown to occur as low as 100 °C.[42] The concentrations of both the F and O decrease during the H_2 anneal.
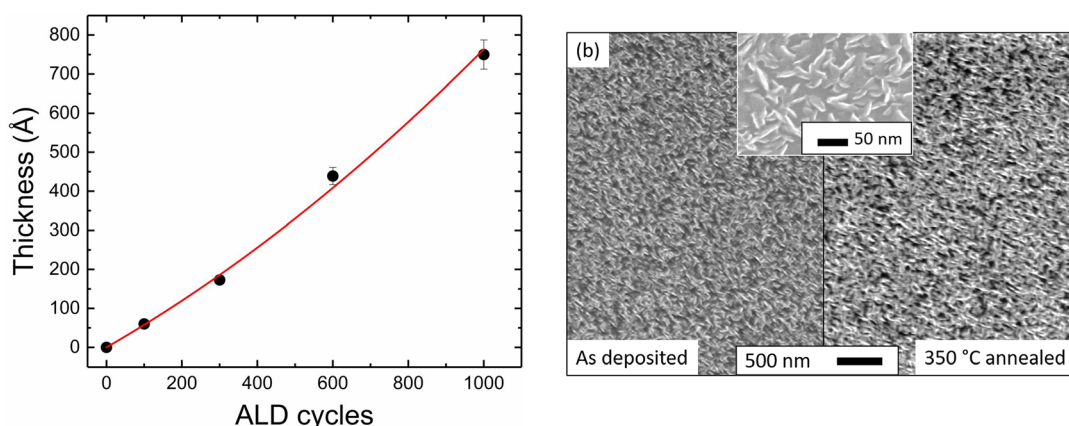

FIG. 3. (Color online) (a) Film thickness as a function of ALD cycles as measured by ellipsometry. (b) SEM image of an as-despoited film after 600 cycles with a thickness of ~45 nm (left) and annealed film (right). The inset shows a higher resolution SEM image of the as-deposited film.
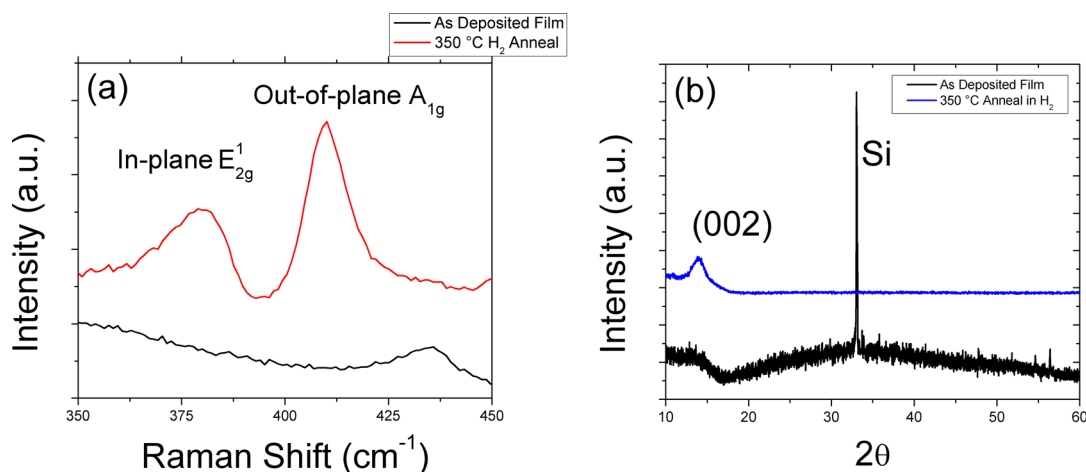
FIG. 4. (Color online) (a) Raman spectroscopy using 514 nm excitation laser showing the as-deposited film (lower), which exhibits a MoS_3 peak at 435 cm^{-1} and the annealed sample (upper) featuring clear MoS_2 fundamental peaks. (b) X-ray diffraction pattern of the as-depostied and annealed sample. After annealing, the (002) reflection associated with the layered structure of MoS_2 is seen.

High-resolution XPS data from the Mo 3d and S 2p regions before and after H_2 anneal are shown in Fig. 6. The energies of the Mo 3d and S 2p peaks were consistent with chemically exfoliated MoS_2 samples.[43] These spectra indicate that there exists MoS_2 and substoichiometric (MoS_x) environments due to the presence of an oxide phase after exposure of the samples to ambient air. The cause for the substoichiometric MoS_2 (MoS_x; where x < 2) is associated with MoS_2 dilution in an oxidized Mo (MoO_x) phase, generating a possible mixed ($Mo-O_x-S_x$) molybdenum oxysulfide species. In fact, oxygen is known to have a high reactivity with the edge defects found in MoS_2 nanoflakes, which are also found in the present work [Fig. 3(b)].[44] Based on the overall composition of Mo and S (Table I), the presence of a mixed Mo(IV) and Mo(V/VI) environment contributes to the small S/Mo ratios of 1.1 and 1.35 for the as-deposited and annealed samples, respectively. Again, this is not surprising given the strong precedence for the stability of MoO_2 and MoO_3 species at temperatures below 550 °C compared to MoS_2, even when sulfurization is undertaken.[45] After analysis of the high-resolution Mo 3d peak envelope [Fig. 6(a)], the integrated peak areas of the peaks corresponding to the

spin-orbit split $3d_{5/2}$ and $3d_{3/2}$ contributions for MoS_2 (~228 and ~231, respectively) relative to the neighboring S-Mo-O_x/$Mo-O_x$ doublet (~229 and ~232 eV, respectively) in the as-deposited and annealed samples increased by 36% and 50%, respectively. Thus, the higher relative amount of MoS_2 after annealing the films in H_2 at 350 °C corroborates the appearance of the (002) diffraction peak in the XRD pattern [Fig. 4(b)], which is characteristic of layered MoS_2. Examination of the high-resolution S 2p XPS peak envelope for both the as-deposited [Fig. 6(c)] and annealed samples [Fig. 6(d)] demonstrates the presence of only S^{2-} with spin-orbit split $2p_{1/2}$ and $2p_{3/2}$ contributions arising at 162.9 and 161.7 eV, respectively.[45,46] It can be concluded that, in addition to removing residual F arising from the MoF_6 precursor, the postannealing procedure was effective in removing some of the oxygen from the stable $Mo-S_x-O_x$ phase, which yielded a purer distribution of MoS_2 with more dominant contributions attributed to Mo(IV) in the Mo 3d XPS region.

To summarize, XRD suggests that the as-deposited film is amorphous whereas the SEM image shows what appear to be nanocrystals. It is likely that the diffraction peaks from these nanocrystals are too weak or broad to be detected by
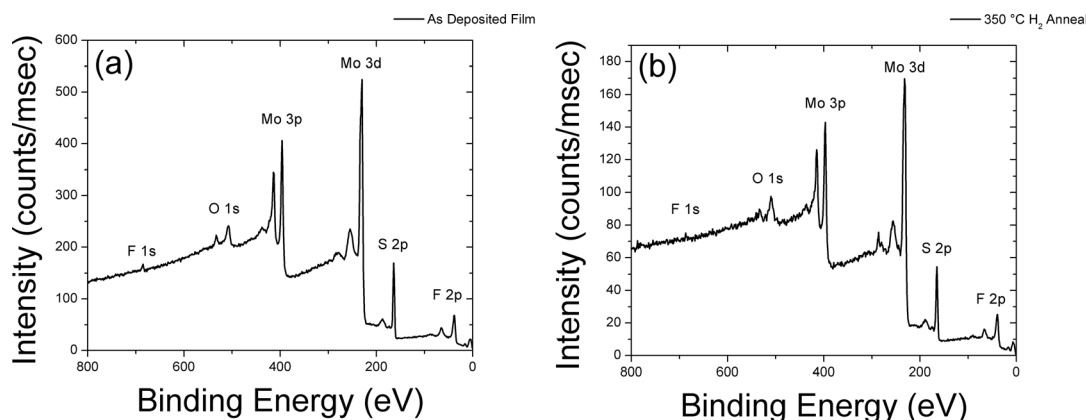

FIG. 5. (a) XPS survey spectra of (a) as-deposited ALD MoS_x film and (b) same film after annealing in H_2.

TABLE I. Atomic percentages as determined by XPS.

Sample	Mo	S	F	O
As-deposited	34.03	37.61	4.37	16.2
Annealed	36.54	48.9	1.22	12.7

our XRD. The Raman measurements do not indicate crystalline MoS_2 as-deposited, and this may result from the residual F detected in the films by XPS. Finally, XPS indicates predominantly Mo(IV), and this agrees with the *in situ* QCM measurements that suggested MoS_2 is the reaction product.

To measure the optical properties of the films, we used fused silica substrates that were masked with Kapton tape preventing deposition from occurring on one side. This process simplified the optical measurements since the beam was only interacting with a single film. Figure 7(a) shows transmission data for ALD MoS_2 films of 12, 32, and 60 nm thickness measured over the visible spectrum in specular transmission mode. Figure 7(b) shows a fit to the 12 nm sample using a Tauc model assuming a direct, allowed transition, and the intercept of this line yields a band-gap of approximately 1.34 eV. This value agrees with literature values for bulk MoS_2.[47]

C. Enhancement of MoS_2 ALD using ZnS

As previously discussed, WS_2 ALD using WF_6 and H_2S can be accelerated by periodically dosing DEZ and H_2S to

form a monolayer of ALD ZnS.[33] To explore whether this same phenomenon occurs during MoS_2 ALD using MoF_6 and H_2S, we performed *in-situ* QCM measurements. Figure 8(a) shows the mass versus time recorded by *in situ* QCM using the timing sequence 1–10-2–10 for the MoS_2 ALD and 1–10-2–10 for the ZnS ALD. In these experiments, two ZnS ALD cycles were performed followed by 20 MoS_2 ALD cycles, and this pattern was repeated several times. As shown in Fig. 8(a), each time the ZnS ALD is performed, the subsequent MoS_2 ALD is enhanced for the next 5–6 cycles and then decreases back to a steady state GPC value of ~0.4 Å/cycle. We note that this behavior is virtually identical to that seen for WS_2 ALD, and the authors speculated that surface Zn might act as a catalyst to reduce the WF_6 and form ZnF, which is converted back to ZnS by exposure to H_2S.

Additional details can be gained from Fig. 8(b) which shows an expanded view of Fig. 8(a) between 9 and 13 cycles as a plot of thickness versus time. The first two ALD ZnS cycles deposit ~2 Å/cycle as expected, but the very first MoS_2 ALD cycle following the ZnS deposits essentially zero mass. The second and third MoS_2 ALD cycles deposit 3.7 and 2.8 Å/cycle, respectively, which are seven to nine times higher than the steady-state value of 0.4 Å/cycle. Moreover, the step shape for these initial MoS_2 ALD cycles are much different from the steady-state step shape shown in Fig. 2(b) indicating different surface chemistry for the MoS_2 ALD half-reactions on the ZnS surface. Previous studies of WS_2
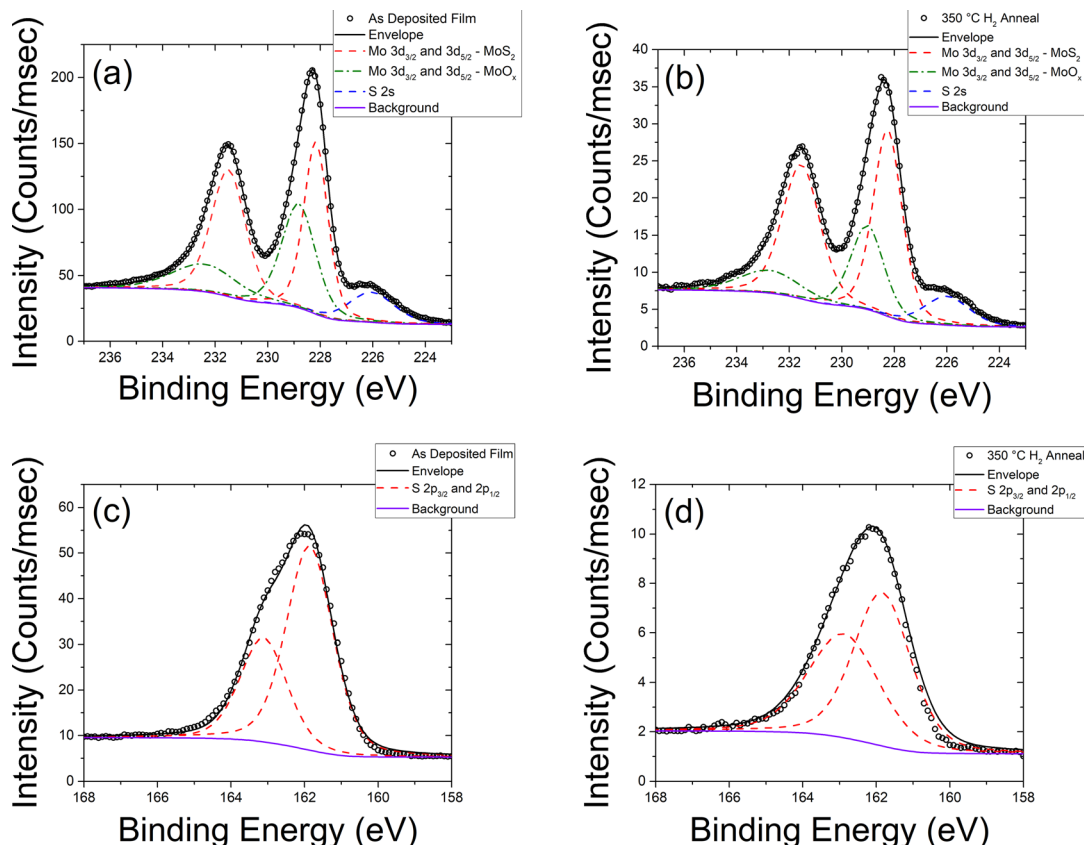

FIG. 6. (Color online) High resolution XPS scans for (a) Mo 3d as deposited, (b) Mo 3d after anneal, (c) S 2p as-deposited, and (d) S 2p after anneal.
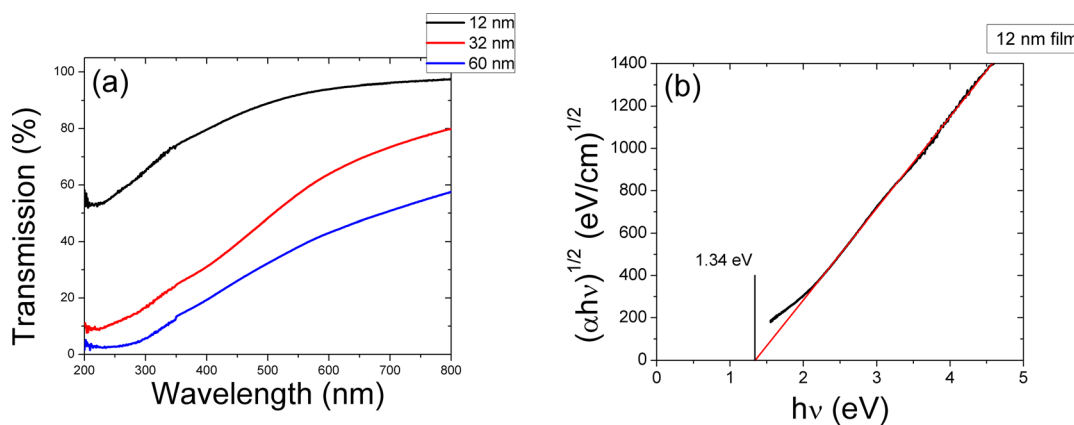
FIG. 7. (Color online) (a) UV-vis transmission measurements of ALD MoS_2 films on fused silica substrates. Clear absorption of the resulting film is seen. (b) Linear regression in the Tauc-plot of the 12 nm sample. A band-gap of approximately 1.3 eV was found.

ALD found ZnF_2 crystals in the WS_2 coating and speculated that reduction of the WF_6 by surface Zn might accelerate the WS_2 ALD.[48] However, this hypothesis fails to account for the first WS_2 ALD cycle, which showed no growth. One explanation for the previous work and the present study is that the initial MoF_6 exposure both adds and removes material from the surface such that the net mass change is nearly zero. For instance, the MoF_6 might react with surface ZnS to yield a volatile sulfide-fluoride compound:

$$ZnS + MoF_6(g) \rightarrow ZnF_2 + MoSF_4(g) + H_2S. \qquad (12)$$

This reaction produces only a 6 amu mass change. Although very little is known about $MoSF_4$, the analogous reaction with ZnO to form $ZnOF_4$ is thermodynamically favorable (-116 kJ/mol at 200 °C), and the $ZnOF_4$ is highly volatile (>1000 Torr at 200 °C). This etching reaction would explain the ZnF_2 residue in the previous papers. Additional in-situ measurements including quadrupole mass spectrometry to identify the gas phase products and Fourier transform infrared (FTIR) absorption spectroscopy to evaluate the surface functional groups directing the surface reactions would help

to understand better the surface chemistry for the ZnS-MoS_2 ALD.

IV. CONCLUSIONS

We have shown using MoF_6 and H_2S as ALD precursors, self-limiting growth of x-ray amorphous MoS_2 is attainable. Two routes of growth were proposed: indirect (MoS_3) and direct (MoS_2). The MoS_3 route is thermodynamically favorable; however, QCM measurement showed that the direct route was the most plausible route. Moreover, XPS data confirmed the as-deposited films were MoS_2. While molybdenum oxide was present, this was attributed to air exposure of the samples upon removal from the reactor at elevated temperature. After hydrogen annealing, crystalline MoS_2 x-ray peaks and Raman peaks were visible.

Similar to the WS_2 accelerated growth on ZnS, DEZ substitution of MoF_6 pulses accelerated the MoS_2 growth. Our QCM measurements suggest that an etching reaction involving volatile $MoSF_4$ species may occur and could explain earlier reports of ZnF_2 residues in WS_2. This work offers an alternative halogen-based process for carbon-free atomic layer deposition of MoS_2 at relatively low temperatures.
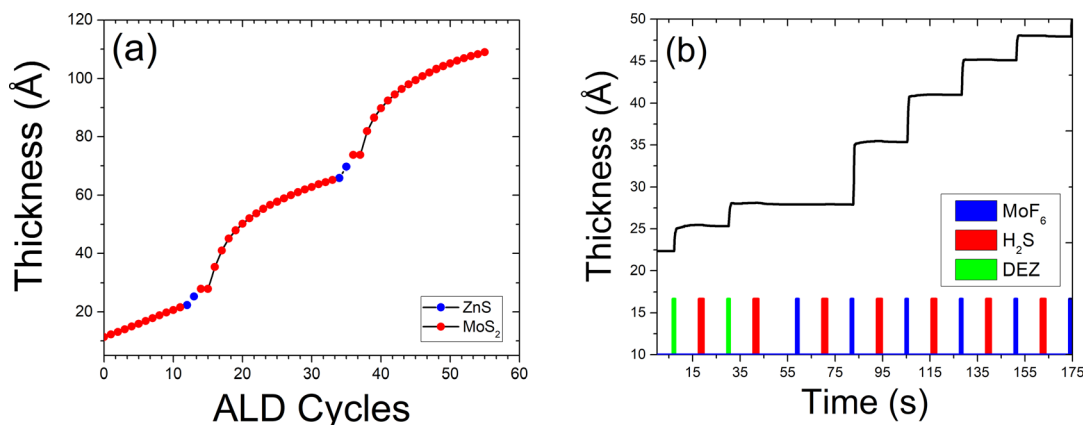

FIG. 8. (Color online) (a) QCM thickness vs ALD cycles for the repeated sequence of 2 cycles ZnS ALD followed by 20 cycles MoS_2 ALD. (b) Expanded view of cycles 9–13 plotted as thickness vs time highlighting the detailed mass changes during the transition from ZnS ALD to MoS_2 ALD. The DEZ, MoF_6, and H_2S dosing times are indicated by the traces at the bottom of the graph.

ACKNOWLEDGMENTS

[1]K. S. Novoselov, A. K. Geim, S. V. Morozov, D. Jiang, Y. Zhang, S. V. Dubonos, I. V. Crigorieva, and A. A. Firsov, Science **306**, 666 (2004).

[2]A. Splendiani, L. Sun, Y. Zhang, T. Li, J. Kim, C. Y. Chim, G. Galli, and F. Wang, Nano Lett. **10**, 1271 (2010).

[3]M. Chhowalla, H. S. Shin, G. Eda, L.-J. Li, K. P. Loh, and H. Zhang, Nat. Chem. **5**, 263 (2013).

[4]T. Spalvins, J. Vac. Sci. Technol., A **5**, 212 (1987).

[5]R. Tenne, Angew. Chem. Int. Ed. **42**, 5124 (2003).

[6]B. Radisavljevic, A. Radenovic, J. Brivio, V. Giacometti, and A. Kis, Nat. Nanotechnol. **6**, 147 (2011).

[7]N. Imanishi, K. Kanamura, and Z. Takehara, J. Electrochem. Soc. **139**, 2082 (1992).

[8]D. K. Nandi, U. K. Sen, D. Choudhury, S. Mitra, and S. K. Sarkar, Electrochim. Acta **146**, 706 (2014).

[9]S. J. Rowley-Neale, D. A. C. Brownson, G. C. Smith, D. A. G. Sawtell, P. J. Kelly, and C. E. Banks, Nanoscale **7**, 18152 (2015).

[10]D. Voiry, M. Salehi, R. Silva, T. Fujita, M. Chen, T. Asefa, V. B. Shenoy, G. Eda, and M. Chhowalla, Nano Lett. **13**, 6222 (2013).

[11]S. Helveg, J. Lauritsen, E. Lægsgaard, I. Stensgaard, J. Nørskov, B. Clausen, H. Topsøe, and F. Besenbacher, Phys. Rev. Lett. **84**, 951 (2000).

[12]R. Dong and I. Kuljanishvili, J. Vac. Sci. Technol. B **35**, 30803 (2017).

[13]A. C. Domask, R. L. Gurunathan, and S. E. Mohney, J. Electron. Mater. **44**, 4065 (2015).

[14]F. Wypych and R. Schöllhorn, J. Chem. Soc., Chem. Commun. **0**, 1386 (1992).

[15]A. O'Neill, U. Khan, and J. N. Coleman, Chem. Mater. **24**, 2414 (2012).

[16]P. Joensen, R. F. Frindt, and S. R. Morrison, Mater. Res. Bull. **21**, 457 (1986).

[17]M. Hegner, P. Wagner, and G. Semenza, Surf. Sci. **291**, 39 (1993).

[18]J. Li, M. M. Naiini, S. Vaziri, M. C. Lemme, and M. Östling, Adv. Funct. Mater. **24**, 6524 (2014).

[19]C. Muratore *et al.*, Appl. Phys. Lett. **104**, 261604 (2014).

[20]C. R. Wu, X. R. Chang, T. W. Chu, H. A. Chen, C. H. Wu, and S. Y. Lin, Nano Lett. **16**, 7093 (2016).

[21]R. A. Vilá, K. Momeni, Q. Wang, B. M. Bersch, N. Lu, M. J. Kim, L. Q. Chen, and J. A. Robinson, 2D Mater. **3**, 41003 (2016).

[22]Y. Feng *et al.*, ACS Appl. Mater. Interfaces **7**, 22587 (2015).

[23]Y. Yu, C. Li, Y. Liu, L. Su, Y. Zhang, and L. Cao, Sci. Rep. **3**, 1866 (2013).

[24]S. M. George, Chem. Rev. **110**, 111 (2010).

[25]L. K. Tan, B. Liu, J. H. Teng, S. Guo, H. Y. Low, and K. P. Loh, Nanoscale **6**, 10584 (2014).

[26]R. Browning, P. Padigi, R. Solanki, D. J. Tweet, P. Schuele, and D. Evans, Mater. Res. Express **2**, 35006 (2015).

[27]A. Valdivia, D. J. Tweet, and J. F. Conley, J. Vac. Sci. Technol., A **34**, 021515 (2016).

[28]J. J. Pyeon, S. H. Kim, D. S. Jeong, S.-H. Baek, C.-Y. Kang, J.-S. Kim, and S. K. Kim, Nanoscale **8**, 10792 (2016).

[29]Y. Jang, S. Yeo, H.-B.-R. Lee, H. Kim, and S.-H. Kim, Appl. Surf. Sci. **365**, 160 (2016).

[30]Z. Jin, S. Shin, D. H. Kwon, S.-J. Han, and Y.-S. Min, Nanoscale **6**, 14453 (2014).

[31]T. Jurca, M. J. Moody, A. Henning, J. D. Emery, B. Wang, J. M. Tan, T. L. Lohr, L. J. Lauhon, and T. J. Marks, Angew. Chem. Int. Ed. **56**, 4991 (2017).

[32]M. Mattinen *et al.*, Adv. Mater. Interfaces **4**, 1700123 (2017).

[33]T. W. Scharf, S. V. Prasad, T. M. Mayer, R. S. Goeke, and M. T. Dugger, J. Mater. Res. **19**, 3443 (2004).

[34]A. Delabie *et al.*, Chem. Commun. **51**, 15692 (2015).

[35]D. Seghete, G. B. Rayner, A. S. Cavanagh, V. R. Anderson, and S. M. George, Chem. Mater. **23**, 1668 (2011).

[36]W. Y. Lee, T. M. Besmann, and M. W. Stott, J. Mater. Res. **9**, 1474 (1994).

[37]W. Y. Lee and K. L. More, J. Mater. Res. **10**, 49 (1995).

[38]N. Lifshitz, D. S. Williams, C. D. Capio, and J. M. Brown, J. Electrochem. Soc. **134**, 2061 (1987).

[39]J. W. Elam, M. D. Groner, and S. M. George, Rev. Sci. Instrum. **73**, 2981 (2002).

[40]H. Li, Q. Zhang, C. C. R. Yap, B. K. Tay, T. H. T. Edwin, A. Olivier, and D. Baillargeat, Adv. Funct. Mater. **22**, 1385 (2012).

[41]W. A. West and A. W. C. Menzies, J. Phys. Chem. **33**, 1880 (1928).

[42]S. Ross and A. Sussman, J. Phys. Chem. **59**, 889 (1955).

[43]G. Eda, H. Yamaguchi, D. Voiry, T. Fujita, M. Chen, and M. Chhowalla, Nano Lett. **11**, 5111 (2011).

[44]A. V. Agrawal, R. Kumar, S. Venkatesan, A. Zakhidov, Z. Zhu, J. Bao, M. Kumar, and M. Kumar, Appl. Phys. Lett. **111**, 93102 (2017).

[45]P. Kumar, M. Singh, R. K. Sharma, and G. B. Reddy, Mater. Res. Express **3**, 55021 (2016).

[46]P. Qin, G. Fang, W. Ke, F. Cheng, Q. Zheng, J. Wan, H. Lei, and X. Zhao, J. Mater. Chem. A **2**, 2742 (2014).

[47]K. K. Kam and B. A. Parkinson, J. Phys. Chem. **86**, 463 (1982).

[48]T. W. Scharf, S. V. Prasad, M. T. Dugger, P. G. Kotula, R. S. Goeke, and R. K. Grubbs, Acta Materialia **54**, 4731 (2006).